

Lappeenranta University of Technology  
School of Engineering Science  
Intelligent Computing Major

Master's Thesis

**Mariia Murashkina**

**CONVEX OBJECT CONTOUR ESTIMATION BASED ON PARTIALLY  
OBSERVED EDGES**

Examiners:      Professor Heikki Kälviäinen  
                     Professor Alexey Potapov

Supervisors:    Professor Heikki Kälviäinen  
                     M.Sc Sahar Zafari  
                     D.Sc Tuomas Eerola  
                     D.Sc Jouni Sampo

# ABSTRACT

Lappeenranta University of Technology  
School of Engineering Science  
Intelligent Computing Major

Mariia Murashkina

## **Convex object contour estimation based on partially observed edges**

Master's Thesis

2017

48 pages, 13 figures, 4 tables, and 2 appendices.

Examiners:      Professor Heikki Kälviäinen  
                         Professor Alexey Potapov

Keywords: image processing, computer vision, machine vision, image segmentation, overlapping objects segmentation, contour estimation, Gaussian processes, active contours, B-splines, ellipse fitting

Segmentation and estimation of overlapping objects aim at automatic analysis of the visible edges to obtain the full contours of objects which can be of different shapes and have different degrees of overlap with each other making the task challenging. This research provides the review and comparison of different existing methods for the contour estimation that rely on the known visible contour points (evidences) and the constraint of convexity for the shape. Based on the comparison results, a new method based on the Gaussian Processes Regression was proposed improving the existing methods which use B-Splines and Ellipse Fitting. The experiments were carried out on a challenging dataset consisting of overlapping nanoparticles and showed the efficiency of the proposed method and its potential over the existing approaches.

# CONTENTS

<b>1</b>	<b>INTRODUCTION</b>	<b>6</b>
1.1	Background . . . . .	6
1.2	Objectives and delimitations . . . . .	7
1.3	Structure of the thesis . . . . .	8
<b>2</b>	<b>SEGMENTATION</b>	<b>9</b>
2.1	Threshold-based segmentation . . . . .	9
2.2	Edge-based segmentation . . . . .	9
2.3	Region-based segmentation . . . . .	9
2.4	Watershed . . . . .	10
2.5	Overlapping objects segmentation . . . . .	10
2.5.1	Segmentation using seedpoint detection . . . . .	10
2.5.2	Ultimate erosion . . . . .	11
2.5.3	Concave points based methods . . . . .	12
<b>3</b>	<b>CONTOUR ESTIMATION AND FITTING</b>	<b>14</b>
3.1	Ellipse-fitting . . . . .	14
3.2	Active contours . . . . .	16
3.3	B-splines . . . . .	19
<b>4</b>	<b>PROPOSED METHOD</b>	<b>21</b>
4.1	Semi-parametric Gaussian process . . . . .	21
4.2	Algorithm description . . . . .	23
<b>5</b>	<b>EXPERIMENTS</b>	<b>27</b>
5.1	Dataset . . . . .	27
5.2	Evaluation criteria . . . . .	27
5.3	Selection of parameters . . . . .	29
5.4	Results . . . . .	30
<b>6</b>	<b>DISCUSSION</b>	<b>36</b>
6.1	Current results . . . . .	36
6.2	Future work . . . . .	37
<b>7</b>	<b>CONCLUSION</b>	<b>39</b>

**REFERENCES****40****Appendices**

Appendix A: Visual results of the SPGP-PF method applied to the ground truth evidences

Appendix B: Visual results of the SPGP-PF method applied to the obtained evidences



## ABBREVIATIONS AND SYMBOLS

ACM	Active Contour Model
BSEM	B-Spline with Expectation Maximization
ECM	Expectation Conditional Maximization
EM	Expectation Maximization
FN	False Negative
FP	False Positive
FRS	Fast Radial Transform
GP	Gaussian Process
JSC	Jaccard Similarity Coefficient
JSI	Jaccard Similarity Index
LSEF	Least-Squares Ellipse Fitting
NURBS	Non-Uniform Rational B-Spline
PPV	Predictive value
SPGP	Semi-Parametric Gaussian Process
SPGP-IPF	Semi-Parametric Gaussian Process with Independent Parametric Form
SPGP-PF	Semi-Parametric Gaussian Process with Polar Form
TP	True Positive
TPR	True Positive Rate

# 1 INTRODUCTION

## 1.1 Background

Object segmentation and detection are among the most common and challenging tasks of image analysis. The most difficult case is when the number of objects is large and they overlap. This is often the case in morphological analysis of medical imagery in registration of cells, organs and other inner parts of the body, and in industrial inspection. To get a better representation of an individual object, its full contour needs to be retrieved. In the case of objects with various degrees of overlapping, there is a very low possibility to observe their full contours which means that there are only partial contours available. The contour estimation process is referred to as contour fitting or approximation. Often no definite assumptions can be made on the shape of the objects making this task difficult. Figure 1 shows the three examples of the overlapping nanoparticles.

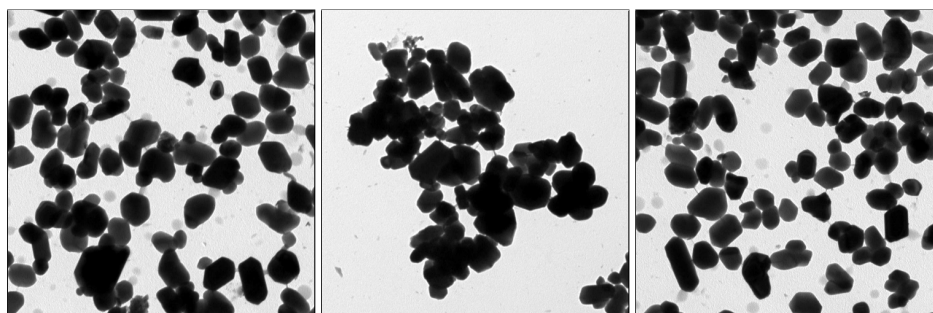


**Figure 1.** Overlapping nanoparticles [1].

This work focuses on the estimation of the full contours of multiple overlapping objects that have convex shape and is based on the previous studies [1, 2, 3, 4]. As proposed in these works, a typical framework for the overlapping convex objects segmentation consists of the following three steps: 1) image preprocessing, 2) contour evidence extraction, and 3) contour estimation. The first step involves identification of the objects, the second step results in grouped sets of the visible contour points for each object, and the last step focuses on the retrieval of the full contour of the objects which is the task addressed in this work. An example of the framework is shown in Figure 2.

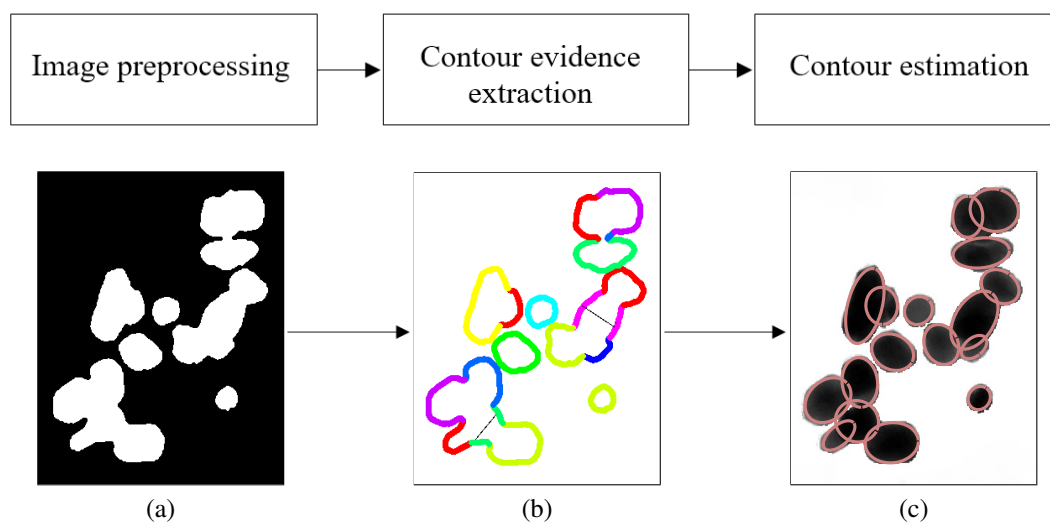


**Figure 2.** Typical steps for overlapping objects segmentation: (a) Binarization; (b) Contour evidences; (c) Contour estimation [2].

## 1.2 Objectives and delimitations

The goals of this research are as follows:

- Provide a survey and comparisons of the existing methods for the contour estimation relying on the known contour points.
- Find the most promising contour estimation methods for overlapping nanoparticles.
- Compare the methods and address their disadvantages by proposing a novel method.

The following delimitations were applied:

- The shape of the objects is predefined to be convex, and no other shapes are considered in this work.
- Image preprocessing and contour evidence extraction implementation are not addressed.

### **1.3 Structure of the thesis**

The remaining part of the thesis is organized as follows. Chapter 2 gives an overview of the existing methods for the general image segmentation and segmentation of overlapping objects. Chapter 3 describes the methods for estimation of the missing contours of occluded objects. Chapter 4 introduces the proposed method for contour estimation. Chapter 5 provides experimental results and comparison of the methods discussed in Chapter 3. Chapter 6 presents discussion of the results as well as future work proposals. Finally, in Chapter 7, the conclusion can be found.

## **2 SEGMENTATION**

Image segmentation is a fundamental problem in image processing and computer vision. Segmentation aims at automatic detection of the areas of interest by partitioning the image into multiple segments based on the properties of the areas. There are three main approaches for image segmentation: pixel-, edge-, and region-based methods [5].

### **2.1 Threshold-based segmentation**

An example of pixel-based methods is thresholding. The segmentation is performed by choosing the threshold value based on the information from the intensities histogram of the image and separating the values which are above or below the threshold value. The most commonly used thresholding method is the Otsu's binarization [6] which adaptively finds an appropriate threshold value for the image.

### **2.2 Edge-based segmentation**

Edge-based segmentation finds and groups edge pixels in the image to form the contour of the objects. The most widely used methods for the contour detection purposes are the Canny [7], Prewitt [8], Sobel [9], and Roberts [10] detectors. They result in an edge map of an image using a certain edge filter. Edges carry significant information about the regions which are separated making this kind of segmentation methods attractive.

### **2.3 Region-based segmentation**

The main idea of the region-based segmentation is dividing an image into certain regions or classes. This group of methods typically takes into account the gray-levels of the adjacent pixels. Region growing [11], split-and-merge [12], and watershed [13] segmentation belong to this group.

The advantages of the region-based methods over the edge-based segmentation are as follows: more information is available to characterize a region, possibility to base the segmentation on the texture of a region and better performance in noisy images where the edges of an object are difficult to detect. On the other hand, edge-based methods generally have lower computational complexity. Both approaches are often coupled to enhance the segmentation performance [5].

## **2.4 Watershed**

Watershed methods are widely used for segmentation purposes. The idea behind the method consists in finding points according to approximate locations of objects and growing a region around them, imitating the process of water filling holes where the holes are the regions. At the point when all the holes are filled up, the boundaries between the regions represent the contours of the objects [5]. Due to its inability to infer invisible parts of the contours, the straightforward watershed technique is not applicable to the overlapping case. However, with some improvements [14] the method can be utilized to segment overlapping objects. The performance of the methods using the watershed transform depends on the initialization and may fail if the number of objects is too large [2]. Also, the marker growing procedure in a watershed method can be noise-sensitive and provide ineffective segmentation [15].

## **2.5 Overlapping objects segmentation**

In the case of partially overlapping objects in an image, there is a high possibility that a straightforward application of traditional segmentation methods fails to distinguish individual objects. Next the methods which consider detection of individual overlapping objects as well as their visible contours extraction, i.e., evidences, are discussed.

### **2.5.1 Segmentation using seedpoint detection**

In [1, 14, 15], the segmentation process consists in identification of seedpoints of individual objects with the further visible contours derivation. Extraction of seedpoints of multiple overlap-

ping objects is an important part of the segmentation process which can influence segmentation accuracy and contour retrieval. The main purpose of the seedpoint extraction is to identify and to count individual objects in the image by assigning seedpoints to each of them. These seedpoints can then be used for the separation of contiguous objects. In [14], they are detected using morphological filtering along with a region growing technique based on intensities followed by the further processing using a watershed-based algorithm for segmentation of occluded cells.

In [1], seedpoints of the objects are extracted using the Fast Radial Transform (FRS) [16] which makes use of the local radial symmetry to highlight the objects of interest in the image. This approach is coupled with the evaluation of the derived seedpoints for their rotational symmetry and convexity. The seedpoints extraction is followed by the edge-to-seedpoint association, during which visible parts of the object's contour are assigned to its seedpoint. This association can be done based on a relevance measure, for example, a cosine distance [15]. Figure 3 shows an example of the contour evidences extraction based on the edge-to-seedpoint association.

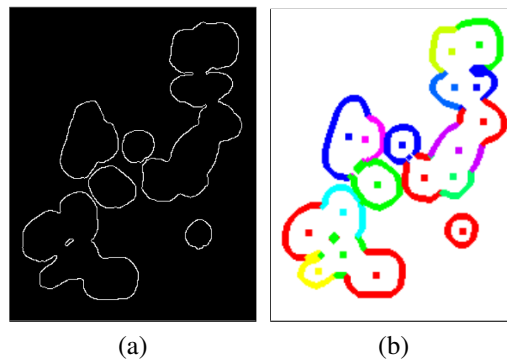


**Figure 3.** Contour evidence extraction using edge-to-seedpoint association: (a) Edges; (b) Association the evidences to the seedpoints (indicated with different colours) [1].

### 2.5.2 Ultimate erosion

Ultimate erosion based segmentation approach makes use of the morphology analysis. In [15], the problem of overlapping nanoparticles segmentation was addressed by a morphological segmentation method and a modified ultimate erosion process for the separation of objects having convex shape. The classical morphological segmentation approach makes use of seedpoints-growing technique. However, in [15] it is modified in a way that edges are assigned to the

detected seedpoints. Identification of the seedpoints is built upon morphological erosion based on the Minkowski subtraction. Erosion results in disconnecting of contiguous or overlapping objects when applied repeatedly. Different stopping criteria can be chosen for this approach; ultimate erosion aims at disconnecting all the objects' groups until they all become separate. Ultimate erosion is generally prone to over-segmentation due to finding several seedpoints instead of one. In [15], this issue is addressed by using an earlier stopping criterion which is more suitable for convex-shaped objects. However, this method can lead to under-segmentation when the degree of overlap is high [1].

### 2.5.3 Concave points based methods

Concave points based approach assumes that the two overlapping convex-shaped objects produce points of contour intersections where their common contour becomes concave. In [2] and [3], this property was utilized to segment individual contour evidences. The first step of segmentation in these methods is getting a binarized (silhouette) image using the Otsu's thresholding [6] followed by extraction of an edge map by the Canny edge detector [7]. After this procedure, concave points are obtained by the detection of the corner points followed by the concavity test. Concave points divide a visible contour into multiple segments, and those belonging to the same object need to be grouped. In [2], the grouping task was solved by utilizing the properties of ellipses, and in [3] the method was improved by applying the branch and bound grouping algorithm. Figure 4 demonstrates the above-mentioned segmentation steps.

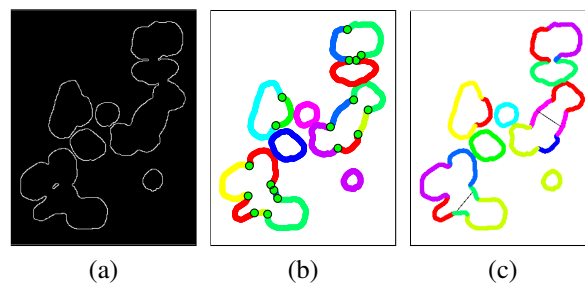


**Figure 4.** Contour segmentation using concave points: (a) Edges; (b) Concave points; (c) Contour segmentation and grouping [2].



In the latest work [17], the concave points detection method from [3] was replaced with a combination of the methods described in [18, 19] which is parameter-free and outperforming the existing methods. Concave points are obtained as follows. Parameter-free polygonal approximation is performed [19] allowing to represent the contours of the objects by a sequence of dominant points and helping to avoid detection of incorrect concave points. The following criteria for the point to be dominant need to be met: the point does not belong to the line connecting the two adjacent points of the sequence and its distance to this line is bigger than a threshold value which is selected automatically. The dominant points are considered concave if they are the connecting points as proposed in [18].

### 3 CONTOUR ESTIMATION AND FITTING

To represent full contours of individual objects, their partial contours retrieved during the segmentation process need to be fitted (approximated) by a curve. The goal is to obtain a contour based on the detected visible edges and assumptions regarding objects' shape. Shapes can vary significantly which makes the fitting task even more complicated. The following subsections describe existing solutions for the task.

#### 3.1 Ellipse-fitting

In [1, 2, 3], the contour estimation task is solved using non-linear ellipse fitting with the classic least square fitting [20] which aims at forming contour parts into an ellipse-shape object. Least square ellipse fitting (LSEF) minimizes the sum of squared algebraic distances from points to an ellipse. An ellipse is represented in a general conic form having six main parameters defining the form and the orientation of an ellipse. The ellipse equation is defined as

$$F(\mathbf{a}, (x, y)) = a_0x^2 + a_1xy + a_2y^2 + a_3x + a_4y + a_5 = \mathbf{a}^T \mathbf{x} = 0, \quad (1)$$

where  $x$  and  $y$  are the input points,  $\mathbf{a} = [a_0 \ a_1 \ a_2 \ a_3 \ a_4 \ a_5]^T$ , and  $\mathbf{x} = [x^2 \ x \ y \ y^2 \ x \ y \ 1]^T$ .

The constraint for the conic to have elliptical form is a negative discriminant value defined as

$$\Delta = a_1^2 - 4a_0a_2 < 0. \quad (2)$$

In the two fundamental researches [20, 21], the fitting problem is addressed through the direct LSEF minimizing the sum  $E$  of the square (algebraic) distance  $d$  from a contour point to an ellipse which are expressed as follows

$$E = \sum_{i=1}^n d^2(\mathbf{a}), \quad (3)$$

$$d(\mathbf{a}) = \sum_{i=1}^N F(x_i, y_i). \quad (4)$$

The task of minimizing  $E$  can be expressed as a solution of an eigenvalue system

$$\mathbf{D}^T \mathbf{D} \mathbf{a} = \lambda \mathbf{C} \mathbf{a}, \quad (5)$$

where  $\mathbf{D} = [\hat{\mathbf{x}}_1 \ \hat{\mathbf{x}}_2 \ \dots \ \hat{\mathbf{x}}_n]^T$ ,  $\hat{\mathbf{x}} = [x^2 \ xy \ y^2 \ x \ y \ 1]$ , and  $\mathbf{C}$  is the matrix representing the discriminant constraint  $\Delta$ . In this case, to represent specifically ellipses and not different second-order conics, the condition in Equation 2 in direct least squares methods is redefined as

$$\Delta = a_1^2 - 4a_0a_2 = -1. \quad (6)$$

The described procedure is summarized in Algorithm 1.

---

**Algorithm 1:** LSEF contour estimation

---

**Input:** Contour evidence points  $x, y$ .

**Output:** Estimated contour  $C$ .

1. Estimate the parameters  $\mathbf{a}$  by minimizing the sum of squared distance  $d$ , Equation 3.
  2. Construct an ellipse according to Equation 1.
- 

Figure 5 shows an example of this method. This approach is a common way to retrieve missing contours of overlapping objects, however, it fails to accurately approximate complicated shapes.

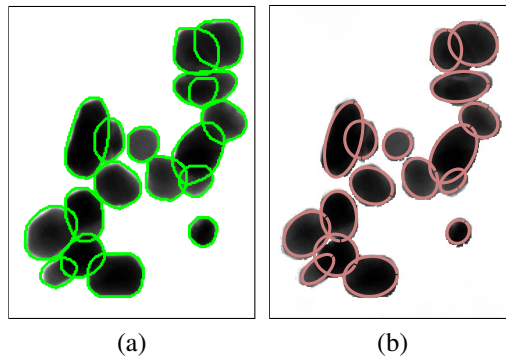


**Figure 5.** Ellipse-fitting example: (a) Ground truth full contours; (b) Ellipse fitting [1].

### 3.2 Active contours

The main idea behind active contour models (ACMs) is to derive a curve to segment an object of interest. According to [15], the ACMs are usually used to segment a single complex-shaped object, and the method is generally unable to operate on multiple overlapping objects. However, the works [22] and [23] address the overlap problem. In [24], the shape prior level-set method is developed which performs better and faster on a small set of objects. ACM can be thought of as an energy-minimizing spline snapping to the important features of the object. They are widely used in many computer vision applications, from line detection to stereo matching [25].

In [23], the following model for multiple occluded objects was used

$$\mathbf{F} = \beta_1 \mathbf{F}_{shape}(\phi, \psi) + \beta_2 \mathbf{F}_{boundary}(\phi, \psi) + \mathbf{F}_{region}(\psi, u_{in}, u_{out}). \quad (7)$$

Given an image  $I : \Omega \rightarrow f$  and the contours  $C \in \Omega$  which divide the image into the foreground  $\Omega_f$  and the background  $\Omega_b$  regions, the contours in the image are represented as a function

$$\phi = \begin{cases} 0 & c \in C \\ -D(c, C) & c \in \Omega_f \\ D(c, C) & c \in \Omega_b \end{cases} \quad (8)$$

where  $D(c, C)$  is the function defining the minimum distance from  $c \in \Omega$  to the contours  $C$ .

The terms in Equation 7 are defined as follows

$$\mathbf{F}_{shape}(\phi, \psi) = \int_{\Omega} (\phi(x, y) - \psi(A(x, y)))^2 dx dy, \quad (9)$$

$$\mathbf{F}_{region}(\psi, u_{in}, u_{out}) = \int_{\Omega} \Theta_{in} \mathbf{H}_{\psi}(x, y) dx dy + \int_{\Omega} \Theta_{out} (1 - \mathbf{H}_{\psi}(x, y)) dx dy, \quad (10)$$

$$\mathbf{F}_{boundary}(\phi, \psi) = \int_{\Omega} g(|\nabla f(x)|) |\psi(x, y)| |\nabla \mathbf{H}_{\psi}(x, y)| dx dy, \quad (11)$$

where

$$\Theta_r = |f(x, y) - c_r|^2 + \mu|\nabla c_r|, \quad r \in \{in, out\},$$

$\mathbf{H}_\psi$  is the Heaviside function,  $g$  is an edge detecting function,  $\beta_1, \beta_2$  are positive constants determining the proportion of each energy functional, and  $\psi$  is the shape prior. The shape prior  $\psi$  can be represented in the form of a single shape or a statistical model considering multiple training shapes. The similarity of the model  $\phi$  and  $\psi$  is defined by a 2-dimensional Euclidean similarity transformation

$$A(x, y) = (s, \theta, T). \quad (12)$$

The shape function  $\mathbf{F}_{shape}$  uses the sum of squared differences between the current contour representation  $\phi(x, y)$  and the adjusted shape prior  $\psi(A(x, y))$  with similarity transformation  $A(x, y)$  as

$$\mathbf{F}_{shape}(\phi, \psi) = \int_{\Omega} (\phi(x, y) - \psi(A(x, y)))^2 dx dy, \quad (13)$$

where  $s, \theta$ , and  $T$  are the scale, rotation, and translation matrices, respectively, performing the affine transformations of the shapes.

Supposing that an image consists of a set of overlapping objects  $\{O_1, O_2, \dots, O_n\}$ , for every pixel  $p(x, y)$  in the image, the rule of assigning it either to one of the objects  $O_i$  or to the background can be expressed as a characteristic function

$$\chi_i = \begin{cases} 1, & p(x, y) \in O_i \\ 0, & \text{otherwise.} \end{cases} \quad (14)$$

Finally, the energy function for segmentation of overlapping objects can be expressed as follows

$$\begin{aligned}
F(\Phi, \Psi, u_{in}, u_{out}) &= \beta_r \int_{\Omega} \Theta_{in} \mathbf{H}_{\vee_{i=1}^n \chi_i}(x, y) dx dy \\
&+ \int_{\Omega} \Theta_{out} (1 - \mathbf{H}_{\vee_{i=1}^n \chi_i}(x, y)) dx dy \\
&+ \beta_2 \sum_{i=1}^n \int_{\Omega} g(|\nabla f(x)|) |\phi_i(x, y)| \nabla \mathbf{H}_{\phi_i}(x, y) dx dy \\
&+ \omega \sum_{i \neq j}^n \int_{\Omega} \mathbf{H}_{\chi_i \wedge \chi_j} dx dy \\
&+ \sum_{i=1}^n \int_{\Omega} \beta_1 (\phi_i(A(x, y)) - \psi(x, y))^2 dx dy, \tag{15}
\end{aligned}$$

where  $\Phi = \{\phi_1, \phi_2, \dots, \phi_n\}$  and  $\Psi = \{\psi_1, \psi_2, \dots, \psi_n\}$  are the sets of curves and shape priors, respectively, and  $\mathbf{H}_{\chi_i \vee \chi_j}$  and  $\mathbf{H}_{\chi_i \wedge \chi_j}$  are

$$\mathbf{H}_{\chi_i \vee \chi_j} = \mathbf{H}_{\phi_i} + \mathbf{H}_{\phi_j} - \mathbf{H}_{\phi_i} \mathbf{H}_{\phi_j}, \quad \mathbf{H}_{\chi_i \wedge \chi_j} = \mathbf{H}_{\phi_i} \mathbf{H}_{\phi_j}. \tag{16}$$

ACMs are able to identify partially observed and imaginary contours, an example of this contour is shown in Figure 6. To perform well, ACMs need to be accurately initialized, and they can be computationally demanding given a large number of objects [2, 7].

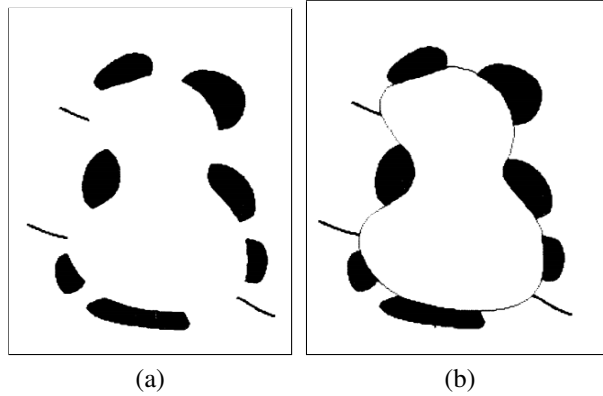


**Figure 6.** Active contours example: (a) Initial image; (b) Estimated contour [25].

### 3.3 B-splines

In [15], both shape classification and contour estimation problems through the construction of a Gaussian mixture model on closed B-splines along with the Expectation Conditional Maximization (ECM) algorithm (BSEM) [26] for the unknown parameters estimation were addressed.

B-spline stands for a basis spline, and it is a polynomial function taking as its parameters the degree of a polynomial  $d$  and the number  $p$  of control points (knots) identifying its shape. The uniform periodic B-spline curve model is defined as follows:

$$f_i(t) = \sum_{i=1}^{p-1} \phi_{h,d}(t) \mathbf{p}_{i,h} \quad (17)$$

where  $\phi_{h,d}(t)$  is the B-spline blending function and  $\mathbf{p}_{i,h}$  is  $h$ th control point. Assuming that the contour evidence data is noisy, the points in the resulting curve  $C = \{c_1, c_2, \dots, c_m\}$  are described by the above model altered by an additive Gaussian noise  $\epsilon$  as

$$c_i = f_i(t_i) + \epsilon_i. \quad (18)$$

The B-spline model construction involves finding the parameters  $t_i$  of the spline (its order and coefficients) as well as the control points  $p_i$  which uniquely describe the output curve. Here, the number of the control points  $p$  and the degree of polynomial  $d$  of the B-spline basis are adjusted by the user, and the parameters  $t_i$  are inferred using a shape-constrained probabilistic model.

The first step of the algorithm is to eliminate the gaps in the partial evidences of the object resulted from the occlusion. This is done by constructing a convex hull of the partial contour points, and the gaps are replaced by a straight line connecting contour parts. The second step is the shape classification of the produced convex hull. The shape of the object is classified based on the predefined training dataset which includes a number of generalized possible objects shapes. This shape assumption is then used to reconstruct the missing parts of the object's contour using maximum likelihood. The whole procedure is described in Algorithm 2.

Having convex-shaped objects which can be thought of as elliptical for simplicity, the minimal number of knots  $p$  can be 4. However, to estimate more complex shapes, the larger  $p$  is preferable. The degree  $d$  of a polynomial basis function can be chosen differently. Cubic splines ( $d \geq 3$ ) are

usually preferred over those with the lower degree, namely linear and quadratic splines, due to the simplicity of representation of the interpolated data along with the smoothness appearance. The main drawbacks of the latter types of splines are discontinuity of the first derivative for linear splines and of the second derivative for quadratic splines. On the other hand, splines of a higher order are prone to contain many extra oscillations [27].

---

**Algorithm 2:** BSEM contour estimation

---

**Input:** Contour evidence points  $x, y$ .

**Output:** Estimated contour  $C$ .

**Parameters:** Number of knots  $p$ , degree of a polynomial  $d$ .

1. Construct a convex hull.
  2. Classify the shape based on the training data.
  3. Estimate the parameters  $t$  using ECM algorithm.
  4. Derive the estimated contour  $C$  according to Equation 17.
-



## 4 PROPOSED METHOD

### 4.1 Semi-parametric Gaussian process

Gaussian process (GP) [28] is a non-parametric model specifying the probability distribution over functions. Similarly to Gaussian probability distribution, it can be completely defined by its two first statistical moments, namely the mean and the covariance functions. In the case of a zero-mean GP, the covariance function completely defines the behaviour of the process, and it specifies the covariance between the two points of the process. The most commonly used covariance functions are [28]:

1. Squared-Exponential:

$$k_{\text{se}}(u, v) = f \exp\left(-\frac{\|u - v\|_2^2}{2l^2}\right) \quad (19)$$

2. Ornstein-Uhlenbeck:

$$k_{\text{ou}}(u, v) = f \exp\left(-\frac{\|u - v\|_2}{l}\right) \quad (20)$$

3. Generally, the Matern covariance function has complicated analytic form including a modified Bessel function of order  $\nu$ . Here are the two most widely used forms of Matern covariance function presented with  $\nu = 3/2$

$$k_{\text{m}3/2} = f \left(1 + \frac{\sqrt{3}\|u - v\|_2}{l}\right) \exp\left(-\frac{\sqrt{3}\|u - v\|_2}{l}\right), \quad (21)$$

and  $\nu = 5/2$

$$k_{\text{m}5/2} = f \left(1 + \frac{\sqrt{5}\|u - v\|_2}{l} + \frac{5\|u - v\|_2^2}{3l^2}\right) \exp\left(-\frac{\sqrt{5}\|u - v\|_2}{l}\right) \quad (22)$$

4. Rational-Quadratic:

$$k_{\text{rq}}(u, v) = f \left(1 + \frac{\|u - v\|_2^2}{2\alpha l^2}\right)^{-\alpha} \quad (23)$$

5. Periodic:

$$k_p(u, v) = f \exp\left(-\frac{2 \sin^2(0.5(u - v))}{l^2}\right) \quad (24)$$

All of the above mentioned covariance functions have two following parameters: the length scale  $l$  and the signal standard deviation  $f$ . The length scale is a measure of the possible distance between the input data and the calculated response to be still correlated.

GP is a widely used model in many areas of machine learning [28]. For the regression, the model known as a semi-parametric GP (SPGP) is commonly used, and it is an extension of GP with standard parametric regression model which can be thought of as a mean function. The SPGP regression model can be formulated as follows

$$\mathbf{y} = h(\mathbf{x})^T \mathbf{w} + f(\mathbf{x}), \quad f \sim \mathcal{GP}(0, k) \quad (25)$$

where  $\mathbf{x}$  and  $\mathbf{y}$  are inputs and outputs of the model, the first term is a parametric part which consists of a set of basis functions  $h(\mathbf{x})$  and parameters  $\mathbf{w}$ , and the second term is a zero-mean Gaussian process with the covariance function  $k$ .

Since SPGP model implies any subset of the function values to be normally distributed, it is possible to use standard formulas for the inference in Gaussian models to predict new output values  $\mathbf{y}^*$  for the new given inputs  $\mathbf{x}^*$  [28]:

$$\mathbf{y}^* = \mathbf{K}_*^T \mathbf{K}^{-1} \mathbf{x} + \mathbf{R}^T \mathbf{w}, \quad (26)$$

$$\mathbf{R} = \mathbf{H}_*^T - \mathbf{H}^T \mathbf{K}^{-1} \mathbf{K}_*, \quad (27)$$

$$\mathbf{w} = (\mathbf{H}^T \mathbf{K}^{-1} \mathbf{H})^{-1} \mathbf{H}^T \mathbf{K}^{-1} \mathbf{x}, \quad (28)$$

where  $(\mathbf{K}_*)_{mn} = k(\mathbf{x}_m^*, \mathbf{x}_n^*)$ ,  $\mathbf{K}_{mn} = k(\mathbf{x}_m, \mathbf{x}_n)$ ,  $\mathbf{H}_{um} = \mathbf{h}(\mathbf{x}_m)$  and  $(\mathbf{H}_*)_{um} = \mathbf{h}(\mathbf{x}_m^*)$ . The above formulas specify all the necessary computations for the regression. To completely determine an SPGP model, it is necessary to define its covariance and basis functions.

Sometimes specifying the type of the covariance function is not enough to get the adequate data prediction [28, 29]. The marginal log likelihood maximization results in a number of possible solutions differently interpreting the data and converges to one of them. If the prediction result is not adequate to the input model, initialization of the kernel function parameters can be performed. Thus, the key to get the desired form of the approximating function is to estimate the nature of

the data accurately. The effect of the kernel function parameters on the prediction is shown in Figure 7 [30].

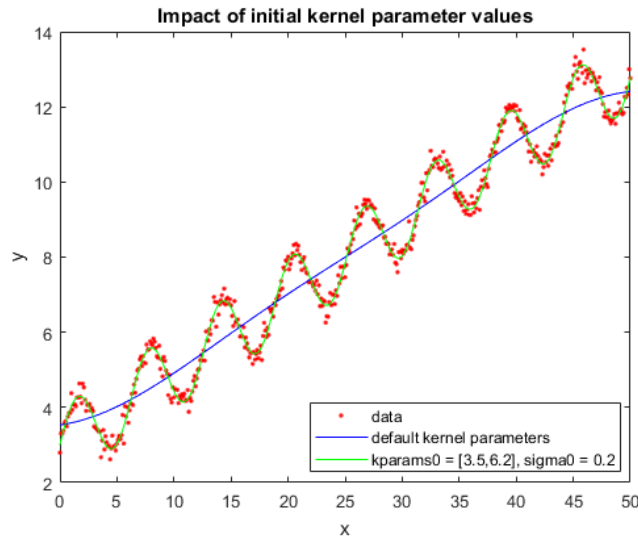


**Figure 7.** Example of the prediction using different kernel functions [30].

## 4.2 Algorithm description

In this work, the SPGP regression model is used for the task of contour estimation. In order to apply this model, it is necessary to define independent and dependent variables. When using the evidence points for the contour estimation in Cartesian coordinates, the experiments showed an issue of extra contour lines going from the intersection point. Figure 8 illustrates an example of this issue.

When using Cartesian coordinates, estimation of the prediction interval is not a trivial task. In absence of the prior knowledge on the size of the object, the search space of the prediction interval is infinite. This issue leads to the following possible solutions: to represent the input data in a polar coordinates form or in a form of parametric curves. The methods described next make use of these two representations which are SPGP with polar form (SPGP-PF) of the evidences and SPGP with independent parametric form (SPGP-IPF).

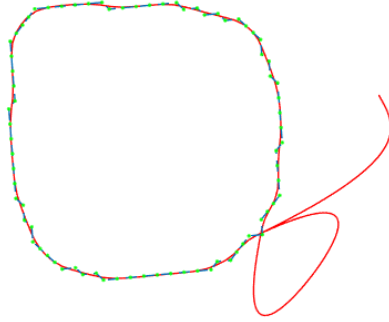


**Figure 8.** Example of wrong prediction interval in case of extra contour lines.

### SPGP-PF

In this method, the problem of estimation of the prediction interval was overcome by means of coordinate system transformation from Cartesian to polar. Given the evidence points  $x$  and  $y$  in Cartesian coordinates, the transformation to polar coordinates can be defined as follows

$$\theta = \arctan\left(\frac{x}{y}\right), \quad (29)$$

$$r = \sqrt{x^2 + y^2}. \quad (30)$$

The result of the transformation is the radial  $r$  and the angular  $\theta$  components. This allows us to fit the function  $r = f(\theta)$  defined on the finite domain  $\theta^* \in [-\pi; \pi]$ .

The input data for the SPGP model consists of the angular and the radial components repeated three times. This is needed for the model to interpret the function  $f(\theta)$  as a closed curve (in Cartesian coordinates) and to learn and predict it accordingly. Thus, the input data can be expressed as

$$\mathbf{x} = \{\theta - 2\pi, \theta, \theta + 2\pi\}, \quad (31)$$

$$\mathbf{y} = \{r, r, r\}. \quad (32)$$

Interpolation can be performed using Equations 26 – 28. The step-by-step description of the method is presented in Algorithm 3.

---

**Algorithm 3: SPGP-PF contour estimation**


---

**Input:** Contour evidence points  $x, y$ .

**Output:** Estimated contour points  $x^*, y^*$ .

**Parameters:** Covariance function  $k$ , parameters  $\mathbf{w}$  of the basis function.

1. Retrieve polar coordinates  $\theta, r$  from  $x, y$  from the center of the points set.
  2. Initialize the input data  $\mathbf{x}, \mathbf{y}$ , Equations 31 – 32.
  3. Perform interpolation of the input data on the interval  $\theta^*$ , Equations 26 – 28.  
The result is the predicted value  $r^*$ .
  4. Transform  $\theta^*, r^*$  from polar to Cartesian coordinates  $x^*, y^*$ .
- 

Generally, for the SPGP-PF, the representation of the input data as a single function  $r = f(\theta)$  results in a form of  $f(\theta)$  which can be difficult to describe analytically, and the choice of the best parameters for the SPGP model is thus not obvious. However, the radius  $r$  comprises the information from both  $x$  and  $y$  components of the evidence points allowing for finding the interpolating model considering the possible correlation between these components.

### SPGP-IPF

An alternative approach is to represent the contour evidences as two independent functions  $f_x$  and  $f_y$  in a parametric form defined as the polar coordinates projections

$$x = f_x(\theta) = r \cos \theta, \quad (33)$$

$$y = f_y(\theta) = r \sin \theta, \quad (34)$$

where  $x$  and  $y$  are the Cartesian coordinates of the evidence points, and  $\theta$  and  $r$  are defined in Equations 29 and 30, respectively. The input data is defined similarly as for the SPGP-PF method

$$\mathbf{x} = \{\theta - 2\pi, \theta, \theta + 2\pi\}, \quad (35)$$

$$\mathbf{y}_x = \{y, y, y\} \quad (36)$$

$$\mathbf{y}_y = \{x, x, x\}. \quad (37)$$

Unlike in the previous approach, the radial component  $r$  is not used since the SPGP model is able to perform the interpolation of  $f_x$  and  $f_y$  based only on the Cartesian coordinates  $x, y$ , and the angular component  $\theta$  defined in Equation 29. The procedure is described in Algorithm 4.

---

**Algorithm 4:** SPGP-IPF contour estimation
 

---

**Input:** Contour evidence points  $x, y$ .

**Output:** Estimated contour points  $x^*, y^*$ .

**Parameters:** Covariance function  $k$ , parameters  $w$  of the basis function.

1. Retrieve the angular component  $\theta$  from the polar coordinates transformation of  $x, y$  from the center of the points set.
  2. Initialize the input data  $\mathbf{x}, \mathbf{y}_x, \mathbf{y}_y$ , Equations 35, 36, 37.
  3. Perform interpolation of the input data on the interval  $\theta^*$ , Equations 26 – 28.  
The result is the predicted values  $x^*, y^*$ .
- 

The representation of the contour evidence as the two functions  $f_x$  and  $f_y$  of the angular parameter  $\theta$  (Equations 33, 34) gives a simply described analytical form of periodical functions, and this may produce more accurate interpolation. However, this representation does not consider the possible correlation between the Cartesian coordinates  $x$  and  $y$  of the evidence points which may result in less efficient contour estimation.

## 5 EXPERIMENTS

### 5.1 Dataset

The dataset consists of 11 real nanoparticles images obtained using a transmission electron microscope. Every image is binarized and contains around 200 particles, represented as dark objects on the white background. Along with the images, the ground truth full contours of the particles are provided. They were manually outlined by an expert and were used during the evaluation process.

Background segmentation and contour evidence extraction were not considered in the experiments. The contour evidences were obtained using the concave-point and branch-and-bound segmentation algorithm proposed in [17] as described in Section 2.5.3. The resulting evidences may have some inaccurately grouped parts representing multiple objects instead of one. This issue may lead to incorrect segmentation and estimation of the contours of these objects. Along with the experimentally obtained evidences, the ground truth evidences were used to evaluate the performance of the contour estimation methods. Example images from the dataset are shown in Figure 9.

### 5.2 Evaluation criteria

For the quantitative method evaluation, three performance measures were used, namely True Positive Rate (TPR), Positive Predictive value (PPV), and Jaccard Similarity Coefficient (JSC). TPR or sensitivity is the percentage of correctly fitted particles, while PPV or precision is the contour estimation accuracy rate. They can be defined as

$$TPR = \frac{TP}{TP + FN} \quad (38)$$

and

$$PPV = \frac{TP}{TP + FP} \quad (39)$$

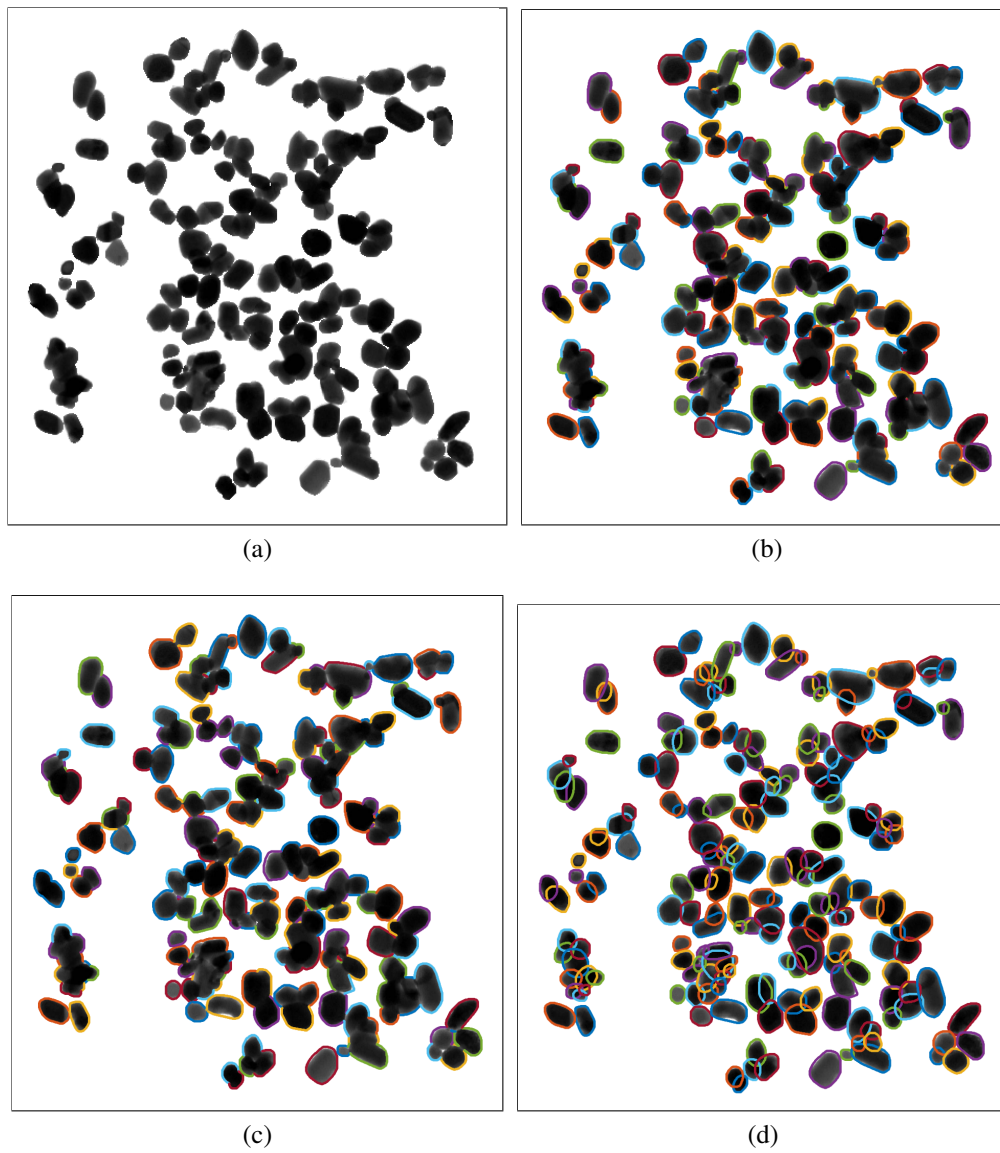


**Figure 9.** Examples of the dataset: (a) Image; (b) Ground truth evidences; (c) Evidences obtained in [17]; (d) Ground truth full contours.



where True Positive (TP) is the number of particles which were segmented correctly, False Positive (FP) is the number incorrectly fitted particles, and False Negative (FN) is the number of missed particles.

The correctness of the contour estimation was measured by the Jaccard Similarity Index (JSI) [31]. It estimates the relation between the area of intersection and the area of union for the pair of the ground-truth contour and the fitted one of each object and is given as

$$JSI = \frac{O_f \cap O_g}{O_f \cup O_g}. \quad (40)$$

where  $O_f$  and  $O_g$  are the areas inside the fitted contour and the ground-truth contour, respectively. Jaccard similarity coefficient is defined as

$$JSC = \frac{TP}{TP + FP + FN} \quad (41)$$

The threshold value for the JSI was chosen to be 0.5 as proposed in [17] and based on the experiments which means that if more than 50% of the object's area is segmented the result is interpreted as positive, or otherwise negative. In the evaluation, the average JSC, TPR, and PPV values were used.

### 5.3 Selection of parameters

#### SPGP

The choice of the covariance function and its parameters is generally not obvious. In this work, for the both SPGP-based methods they were chosen empirically based on the experimental results. Table 1 presents the parameters for the SPGP method set in the experiments.

**Table 1.** Selected parameters for SPGP.

Parameter	Value
Covariance function	Matern 3/2
Basis function	Constant: $h = 1$

## BSEM

The algorithm requires the adjustment of the B-spline parameters, the degree of a polynomial  $d$  and the number of control points  $p$ . They are set to the default values as proposed in [15] and are presented in Table 2.

**Table 2.** Selected parameters for BSEM.

Parameter	Value
Degree of a polynomial	$d = 4$
Number of control points	$p = 8$

## LSEF

For the LSEF method, no parameters tuning is needed.

## 5.4 Results

The performance of the contour estimation methods, namely SPGP-PF, SPGP-IPF, BSEM, and LSEF, was evaluated using both the ground truth contour evidences and the evidences obtained with the method from [17] as an input. The performance comparison of the three methods was estimated by the average values of TPR, PPV, and JSC. Table 3 shows the estimates of the performance on the ground truth evidences, while Table 4 presents the performance estimates for the methods applied to the evidences from [17]. Figures 10 and 11 show the visual results of the methods applied to the ground truth evidences and to the evidences from [17] compared to the ground truth full contour. Figures 12 and 13 present the evaluation results for the methods in terms of TPR, PPV, and JSC with the different JSI threshold values. The visual results of the proposed SPGP-PF method on all the images from the ground truth evidences dataset and from the evidences obtained in [17] are given in Appendix A and Appendix B, respectively.

**Table 3.** The performance of the contour estimation methods on the ground truth contour evidences.

Method	TPR [% ]	PPV[%]	JSC [%]
SPGP-PF	98	97	95
SPGP-IPF	92	91	84
BSEM	94	94	89
LSEF	95	96	92

**Table 4.** The performance of the contour estimation methods on the contour evidences from [17].

Method	TPR [% ]	PPV[%]	JSC [%]
SPGP-PF	90	83	77
SPGP-IPF	84	78	68
BSEM	87	81	72
LSEF	89	85	77

According to the evaluation results, all the methods achieved satisfactory segmentation results on the both parts of the dataset, with the SPGP-PF method showing better performance on the ground truth evidences. From Figure 10, it can be seen that the BSEM and SPGP-IPF methods tend to underestimate the shape of the objects with small contour evidences resulting in a narrow shape, while LSEF can result in larger shapes. It should be mentioned that evidences with less than two points (about 2% of the data) were left out since such low amount of points cannot provide adequate information on the shape of the object. In Figure 11 the estimation inaccuracy can be seen which is due to the wrong grouping of the evidences resulting in multiple objects instead of one.

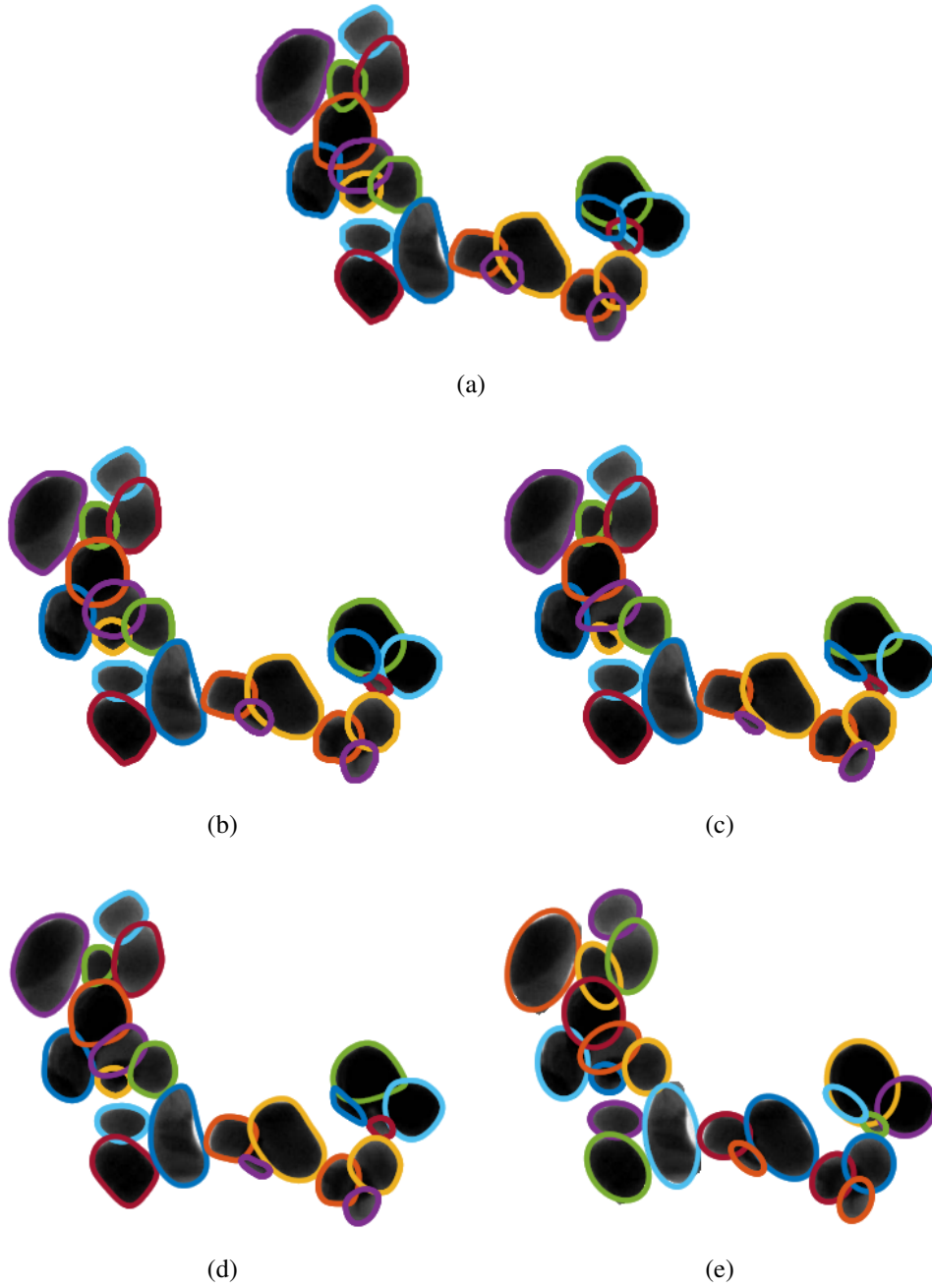


**Figure 10.** Contour estimation results on the ground truth dataset: (a) Ground truth full contour; (b) SPGP-PF; (c) SPGP-IPF; (d) BSEM; (e) LSEF.

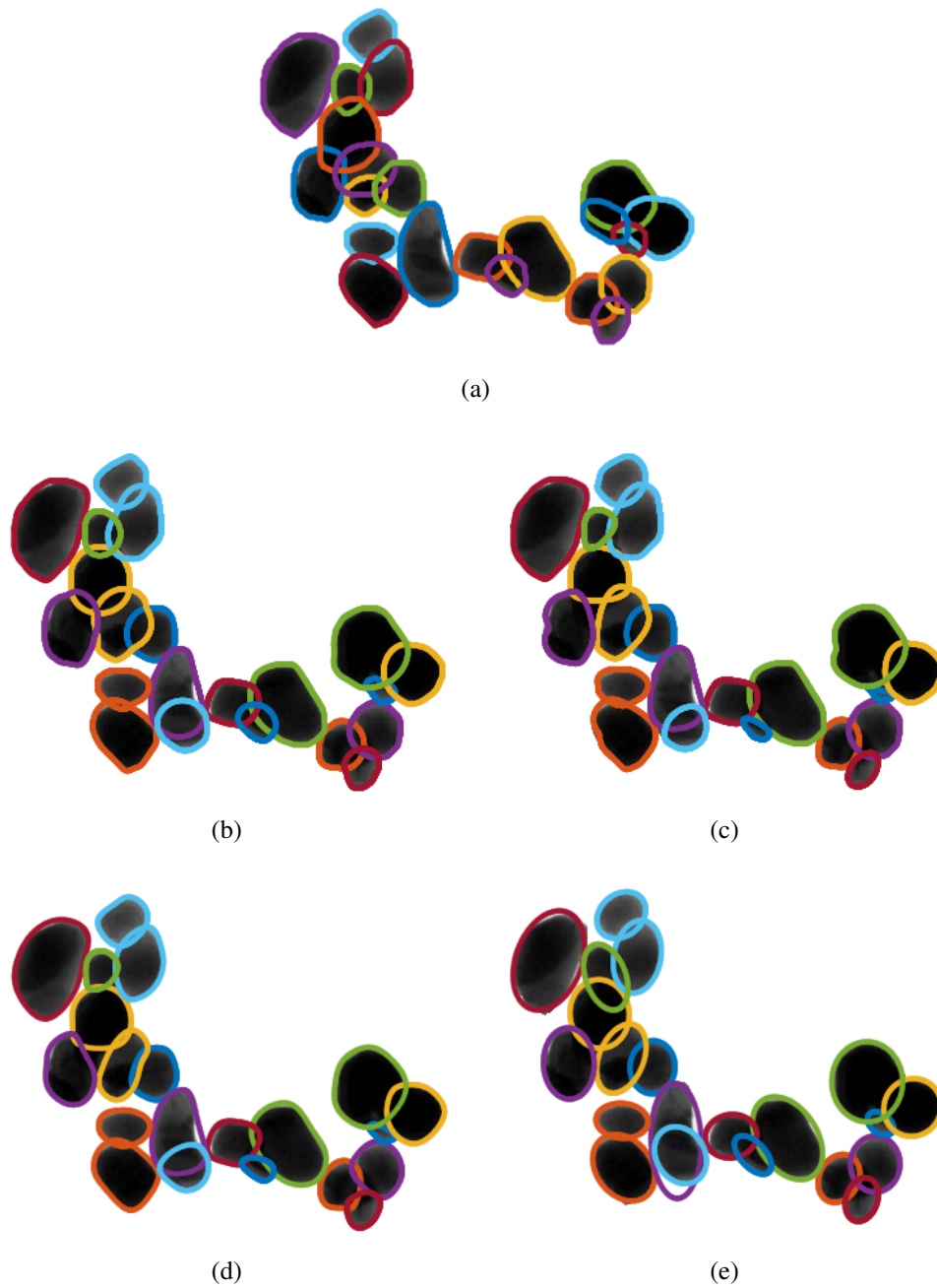


**Figure 11.** Contour estimation results on the evidences from [17]: (a) Ground truth full contour; (b) SPGP-PF; (c) SPGP-IPF; (d) BSEM; (e) LSEF.

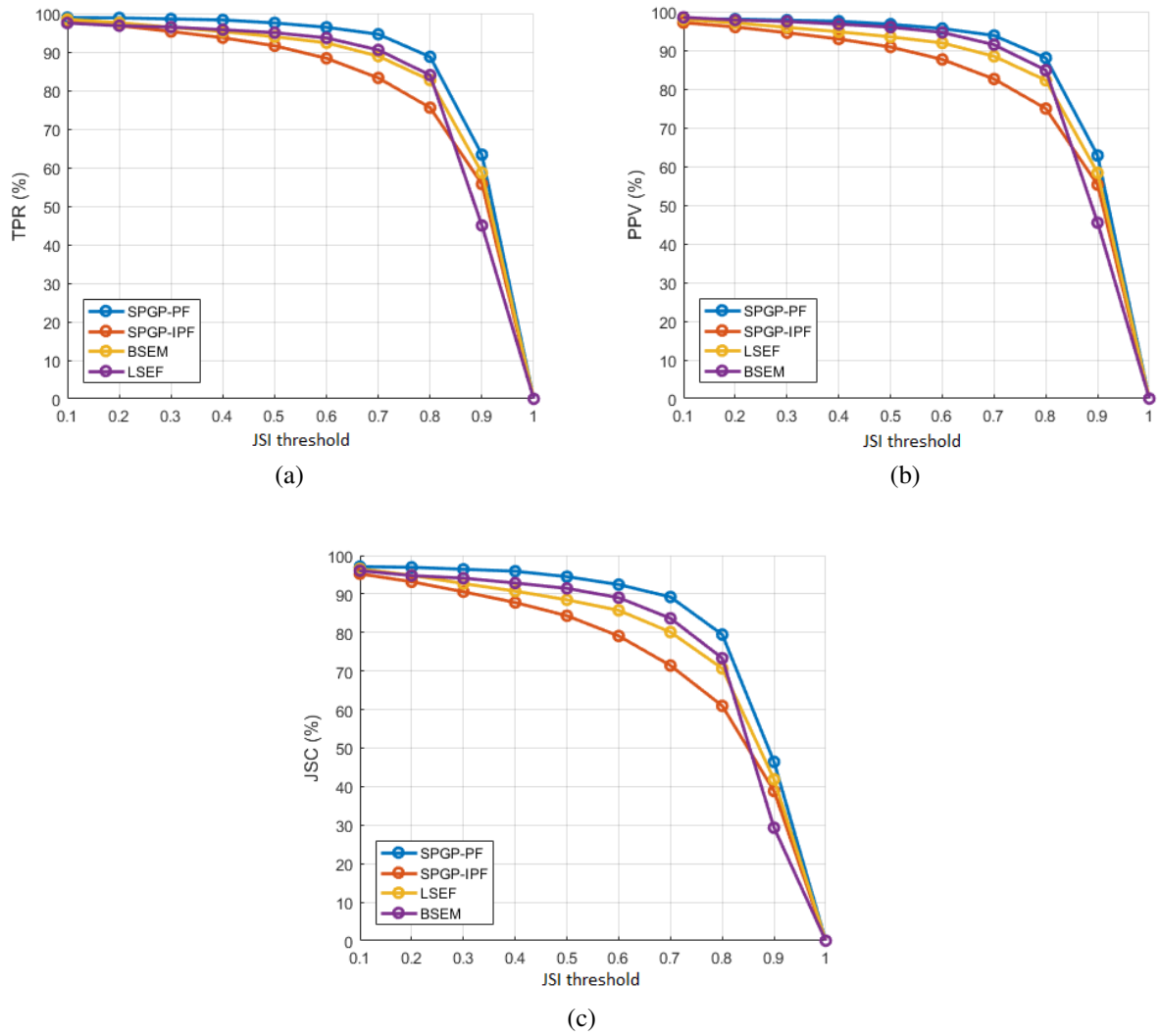


**Figure 12.** Evaluation results for the methods with the different JSI threshold value applied to the ground truth evidences: (a) TPR; (b) PPV; (c) JSC.

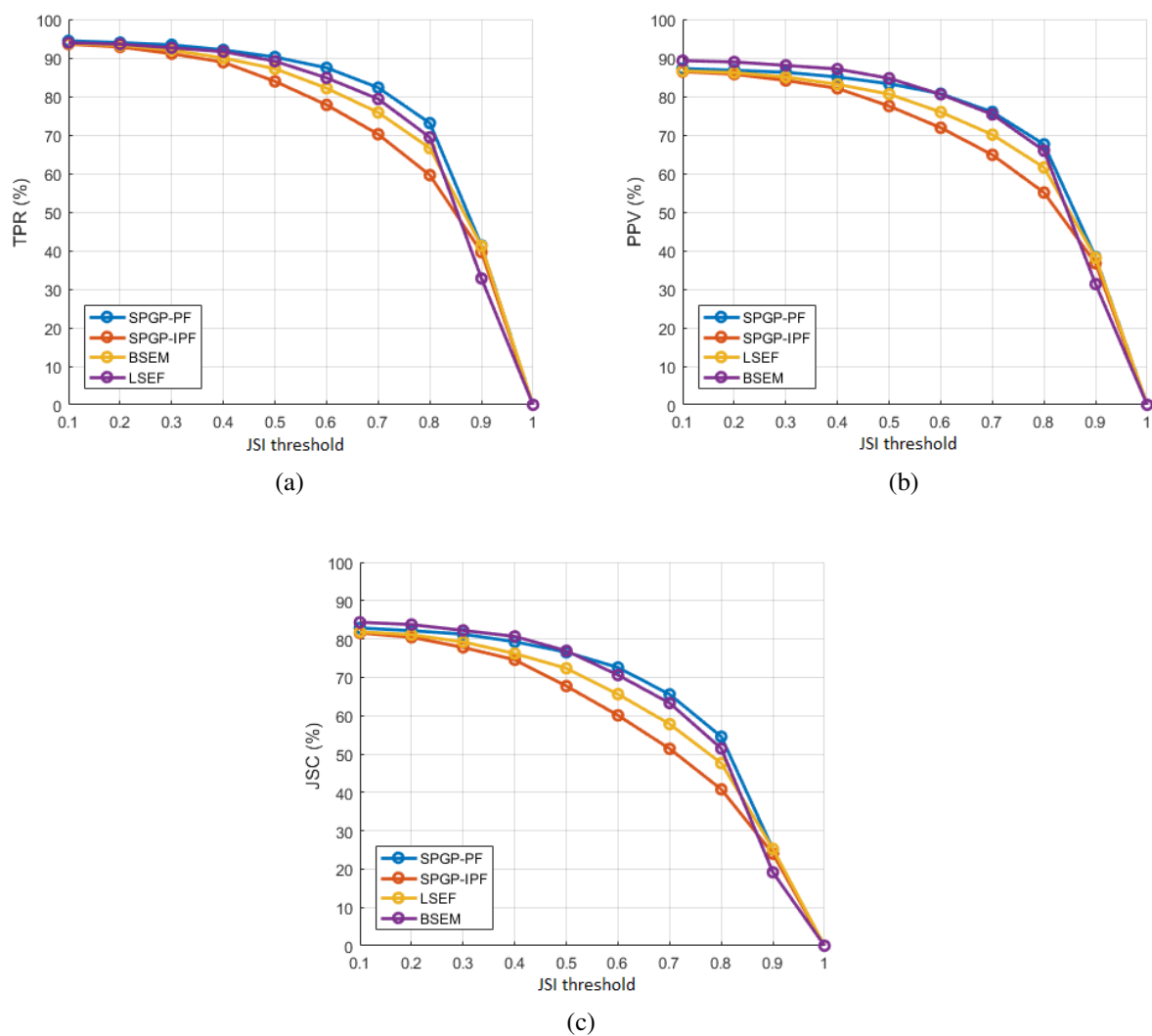


**Figure 13.** Evaluation results for the methods with the different JSI threshold value applied to the evidences from [17]: (a) TPR; (b) PPV; (c) JSC.

## 6 DISCUSSION

### 6.1 Current results

The task of overlapping objects segmentation and estimation of their full contour has been among the complicated ones in the scope of image processing. This problem may arise in different possible applications, from industrial inspection to medical imaging where many small particles need to be detected and counted, e.g., nanoparticles or cells. The work presents a new method for the contour estimation based on the visible partial evidences as well as the comparison with the two state-of-the-art methods.

The comparison of the existing contour estimation methods showed the demand for a new approach overcoming the drawbacks of these methods. The proposed contour estimation method is based on the semi-parametric Gaussian process regression (SPGP) model aiming at interpolation of the partial evidence contour of an object. Reconstruction of the full contours of the object was based on the visible partial evidences. The experiments were carried out on the ground truth evidences provided by an expert and on the evidences obtained from the method described in [17].

The performance of the proposed method was evaluated on the both evidences datasets and showed good results. The comparison with two other existing approaches, B-splines with expectation maximization (BSEM) [15] and direct least-square ellipse fitting (LSEF) [20] revealed the potential of the proposed method (SPGP) in the means of accuracy of the contour estimation and ability to estimate the full contour of the object. The performance measurements on the ground truth evidences dataset were as follows: the average TPR of 98%, PPV of 97%, and JSC of 95%. On the evidences obtained in [17], the corresponding performance results were as follows: 90%, 83%, and 77%.

The experiments showed that the SPGP-PF method has better performance compared to the SPGP-IPF. Initially, the choice of the input data representation was not obvious, and thus in this work these two options were analysed. For the SPGP-IPF, most of the commonly used covariance functions produced the accurate interpolation for both functions  $f_x$  and  $f_y$ . However, since the method does not consider the possible correlation between  $x$  and  $y$ , it predicts the missing parts of the evidence less accurately.



## 6.2 Future work

Possible improvements and modifications of the proposed method can be suggested. The framework for objects segmentation and contour estimation consists of the following parts: Contour Evidence Extraction, Contour Estimation, and Evaluation. Each part is independent from the others and is a matter for further development.

The accuracy of the evidence extraction procedure is crucial for the overall model performance. The contour evidence extraction was performed using the method proposed in [17]. It consists of the two parts: segmentation of the visible contour resulting in separate segments, and grouping of the segments belonging to the same object. While the segmentation part of the method provides comparatively accurate results [17], the results of the grouping part can be improved. The following issue was discovered: the grouping part of the method sometimes treats the contour segments of one object as if they belong to different objects. This shortcoming increases the overall segmentation inaccuracy since there are more objects detected than there are present in the image.

The proposed contour estimation method uses the Gaussian processes model. Being flexible to the variations in the form of the interpolated function (contour evidence), SPGP gives good results on the provided nanoparticles datasets. However, in different applications, the shapes of the objects can vary significantly and a more suitable interpolation model might be desirable. The performance of the method is influenced by the parameters mentioned in Section 4.1, and they can be chosen more carefully based on the analysis of the contour evidence shape. The choice of the covariance and the basis functions is one of the most important factor influencing to the performance of the method, and it should be based on the analysis of the form of the input data. In this work, one of the commonly used covariance functions was utilized which produced adequate results in the experiments. However, more in-depth research on the SPGP parametrization can be carried out to address different kinds of problems. More details can be found in [28] and [29]. The SPGP-IPF method can be improved by the regulation to the prior shape (a training dataset) to better infer the missing parts of the contour, however, the methods utilizing it (BSEM, ACM) can be limited to those shapes and be unable to produce the contours of the different shapes.

The contour estimation methods were evaluated on 11 microscopic images each containing ap-

proximately 200 overlapping nanoparticles. To verify the applicability of the proposed method to the various cases, it would be beneficial to evaluate the methods on other image datasets representing the objects of different nature, shapes, and occlusions captured using various imaging settings.

## 7 CONCLUSION

In this thesis, different methods for segmentation of the overlapping objects of convex shape were studied. The general framework includes image segmentation, contour evidence extraction, and contour estimation. The main focus of this work was to address the problem of the last step, and the state-of-the-art methods were studied and compared. The performance of the methods was evaluated on a set of real nanoscale images with provided contour evidence dataset. This dataset consisted of the two parts: the ground truth outlined by an expert and the data obtained from the related research on contour evidence extraction explained in [17].

In order to improve the existing contour estimation methods, the new method was proposed based on the Semi-Parametric Gaussian Processes (SPGP) regression model. Given the partial contour evidence points of each object, the method aims at estimation of its full contour and inferring the missing contour parts.

The efficiency of the proposed method was verified through its comparison with the other two existing contour estimation methods, namely B-Splines with Expectation Maximization (BSEM) and direct Least Square Ellipse Fitting (LSEF). The experiments demonstrated the efficiency and reliability of the proposed method as well as its potential over the existing approaches.

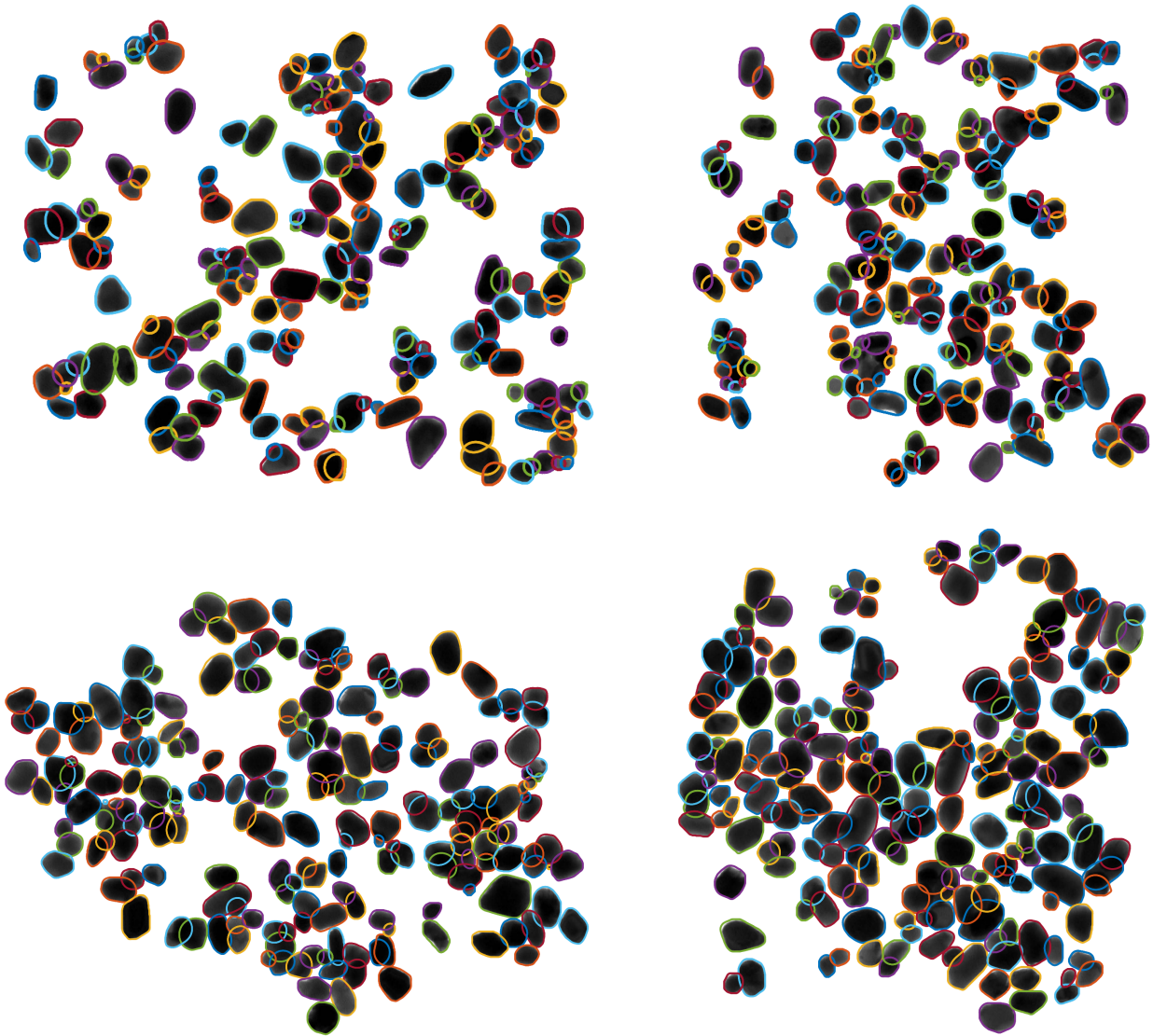
## REFERENCES

- [1] Sahar Zafari, Tuomas Eerola, Jouni Sampo, Heikki Kälviäinen, and Heikki Haario. Segmentation of overlapping elliptical objects in silhouette images. *IEEE Transactions on Image Processing*, 24(12):5942–5952, 2015.
- [2] Sahar Zafari, Tuomas Eerola, Jouni Sampo, Heikki Kälviäinen, and Heikki Haario. Segmentation of partially overlapping nanoparticles using concave points. In *Advances in Visual Computing*, volume 9474 of *Springer Lecture Notes in Computer Science, LNCS. Proceedings of International Symposium on Visual Computing (ISVC)*, pages 187–197. Springer, 2015.
- [3] Sahar Zafari, Tuomas Eerola, Jouni Sampo, Heikki Kälviäinen, and Heikki Haario. Segmentation of partially overlapping convex objects using branch and bound algorithm. In *ACCV 2016: Computer Vision – ACCV 2016 Workshops*, volume 10118 of *Springer Lecture Notes in Computer Science, LNCS. Proceedings of ACCV Workshop Mathematical and Computational Methods in Biomedical Imaging and Image Analysis (MCBMIIA2016)*, pages 76–90. Springer, 2017.
- [4] Sahar Zafari. Segmentation of overlapping convex objects. Master’s thesis, Lappeenranta University of Technology, 2014.
- [5] Fritz Albregtsen. Region- and edge-based segmentation. <http://www.uio.no/studier/emner/matnat/ifi/INF4300/h11/undervisningsmateriale/INF4300-2011-f04-segmentation.pdf>, 2011. [Online; Accessed May - 2017].
- [6] Nobuyuki Otsu. A threshold selection method from gray-level histograms. *Automatica*, 11(285-296):23–27, 1975.
- [7] John Canny. A computational approach to edge detection. *IEEE Transactions on Pattern Analysis and Machine Intelligence*, 8(6):679–698, nov 1986.
- [8] Judith MS Prewitt. Object enhancement and extraction. *Picture Processing and Psychopictorics*, 10(1):15–19, 1970.
- [9] N Senthilkumaran and R Rajesh. Edge detection techniques for image segmentation—a survey of soft computing approaches. *International Journal of Recent Trends in Engineering*, 1(2):250–254, 2009.

- [10] Lawrence Gilman Roberts. *Machine Perception of Three-Dimensional Soups*. PhD thesis, Massachusetts Institute of Technology, 1963.
- [11] Rolf Adams and Leanne Bischof. Seeded region growing. *IEEE Transactions on Pattern Analysis and Machine Intelligence*, 16(6):641–647, 1994.
- [12] S. L. Horowitz and T. Pavlidis. Picture Segmentation by a directed split-and-merge procedure. *Proceedings of the 2nd International Joint Conference on Pattern Recognition*, pages 424–433, 1974.
- [13] Fernand Meyer and Serge Beucher. Morphological segmentation. *Journal of Visual Communication and Image Representation*, 1(1):21–46, 1990.
- [14] Jie Shu, Hao Fu, Guoping Qiu, Philip Kaye, and Mohammad Ilyas. Segmenting overlapping cell nuclei in digital histopathology images. In *35th Annual International Conference of the IEEE Engineering in Medicine and Biology Society (EMBC)*, pages 5445–5448. IEEE, 2013.
- [15] Chiwoo Park, Jianhua Z Huang, Jim X Ji, and Yu Ding. Segmentation, inference and classification of partially overlapping nanoparticles. *IEEE Transactions on Pattern Analysis and Machine Intelligence*, 35(3):1–1, 2013.
- [16] Gareth Loy and Alexander Zelinsky. Fast radial symmetry for detecting points of interest. *IEEE Transactions on Pattern Analysis and Machine Intelligence*, 25(8):959–973, 2003.
- [17] Sahar Zafari, Tuomas Eerola, Jouni Sampo, Heikki Kälviäinen, and Heikki Haario. Comparison of concave point detection methods for overlapping convex objects segmentation. In *Proceedings of Scandinavian Conference on Image Analysis*. Springer, 2017.
- [18] Wen-Hui Zhang, Xiaoya Jiang, and Yin-Mingzi Liu. A method for recognizing overlapping elliptical bubbles in bubble image. *Pattern Recognition Letters*, 33(12):1543–1548, 2012.
- [19] Dilip K Prasad and Maylor KH Leung. *Polygonal representation of digital curves*. INTECH Open Access Publisher, 2012.
- [20] Andrew Fitzgibbon, Maurizio Pilu, and Robert B Fisher. Direct least square fitting of ellipses. *IEEE Transactions on Pattern Analysis and Machine Intelligence*, 21(5):476–480, 1999.

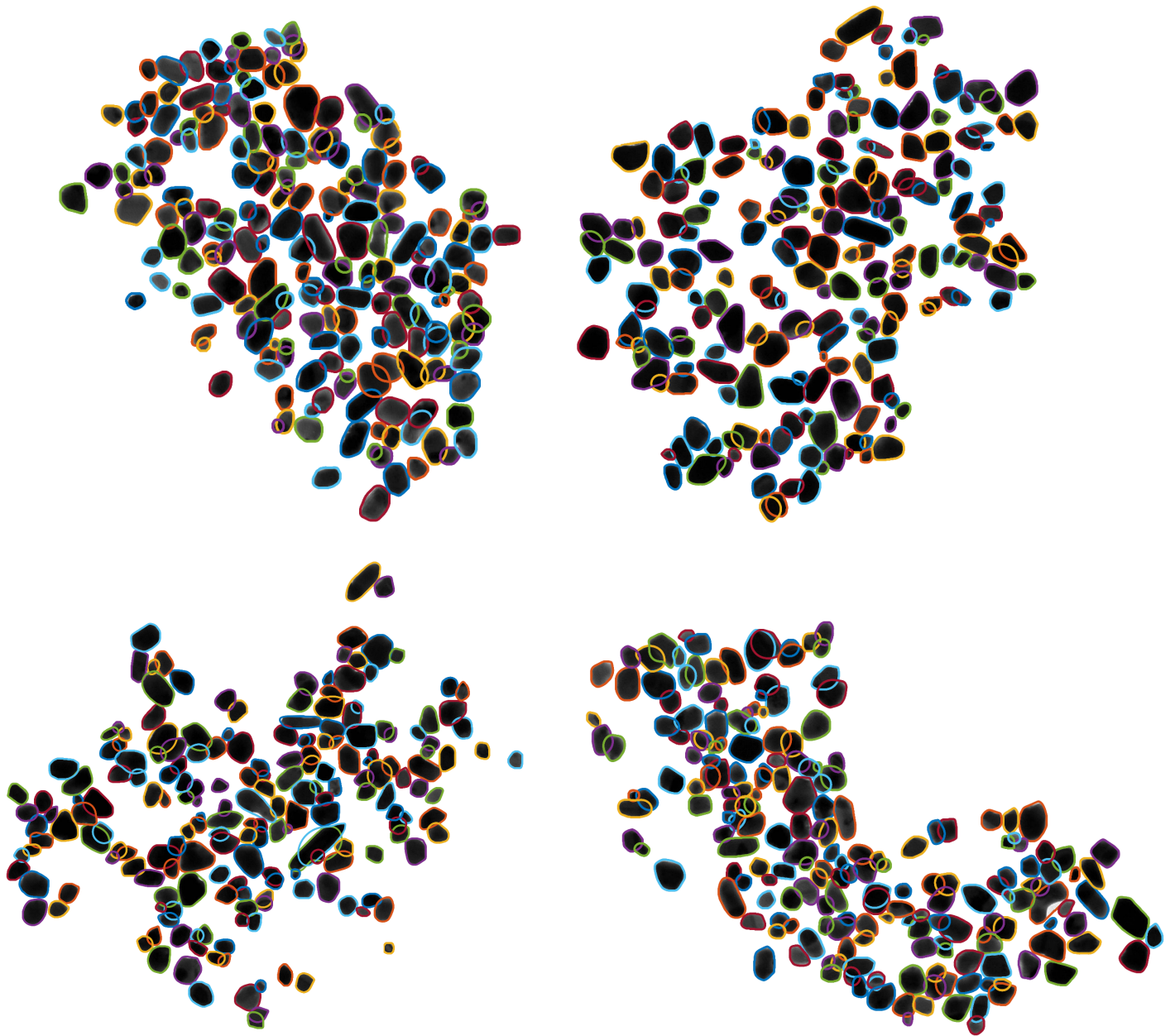
- [21] Maurizio Pilu, Andrew W Fitzgibbon, and Robert B Fisher. Ellipse-specific direct least-square fitting. In *Proceedings of International Conference on Image Processing*, volume 3, pages 599–602. IEEE, 1996.
- [22] Qilong Zhang and Robert Pless. Segmenting multiple familiar objects under mutual occlusion. In *IEEE International Conference on Image Processing (ICIP)*, pages 197–200, 2006.
- [23] Sahirzeeshan Ali and Anant Madabhushi. An integrated region-, boundary-, shape-based active contour for multiple object overlap resolution in histological imagery. *IEEE Transactions on Medical Imaging*, 31(7):1448–1460, 2012.
- [24] Yunmei Chen, Hemant D Tagare, Sheshadri Thiruvankadam, Feng Huang, David Wilson, Kaundinya S Gopinath, Richard W Briggs, and Edward A Geiser. Using prior shapes in geometric active contours in a variational framework. *International Journal of Computer Vision*, 50(3):315–328, 2002.
- [25] Michael Kass, Andrew Witkin, and Demetri Terzopoulos. Snakes: Active contour models. *International Journal of Computer Vision*, 1(4):321–331, 1988.
- [26] Xiao-Li Meng and Donald B Rubin. Maximum likelihood estimation via the ecm algorithm: A general framework. *Biometrika*, 80(2):267–278, 1993.
- [27] Splines and piecewise interpolation. <http://citeseerx.ist.psu.edu/viewdoc/download?doi=10.1.1.713.6275&rep=rep1&type=pdf>. [Online; Accessed May - 2017].
- [28] Christopher KI Williams and Carl Edward Rasmussen. Gaussian processes for machine learning. *MIT Press*, 2(3):4, 2006.
- [29] David Duvenaud, James Robert Lloyd, Roger Grosse, Joshua B Tenenbaum, and Zoubin Ghahramani. Structure discovery in nonparametric regression through compositional kernel search. In *Proceedings of the International Conference on Machine Learning, ICML*, volume 28, pages 1166–1174, 2013.
- [30] Matlab documentation on the gaussian process regression (fitrgp). <https://www.mathworks.com/help/stats/fitrgp.html>. [Online; Accessed May - 2017].
- [31] Seung seok Choi and Sung hyuk Cha. A survey of binary similarity and distance measures. *Journal of Systemics, Cybernetics and Informatics*, 8(1):43–48, 2010.

**Appendix A. Visual results of the SPGP-PF method applied to the ground truth evidences**



(continues)

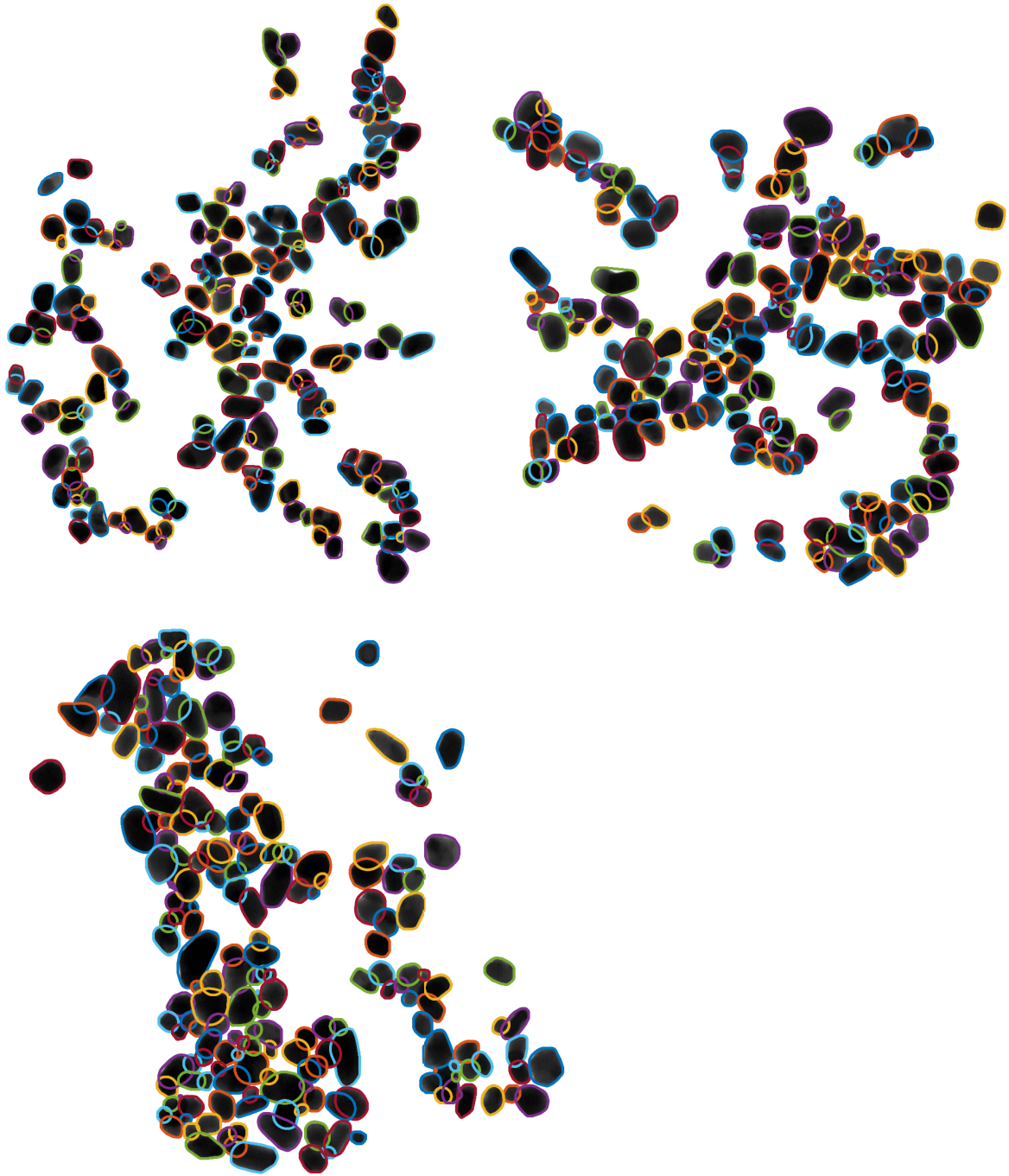
Appendix A. (continued)



(continues)

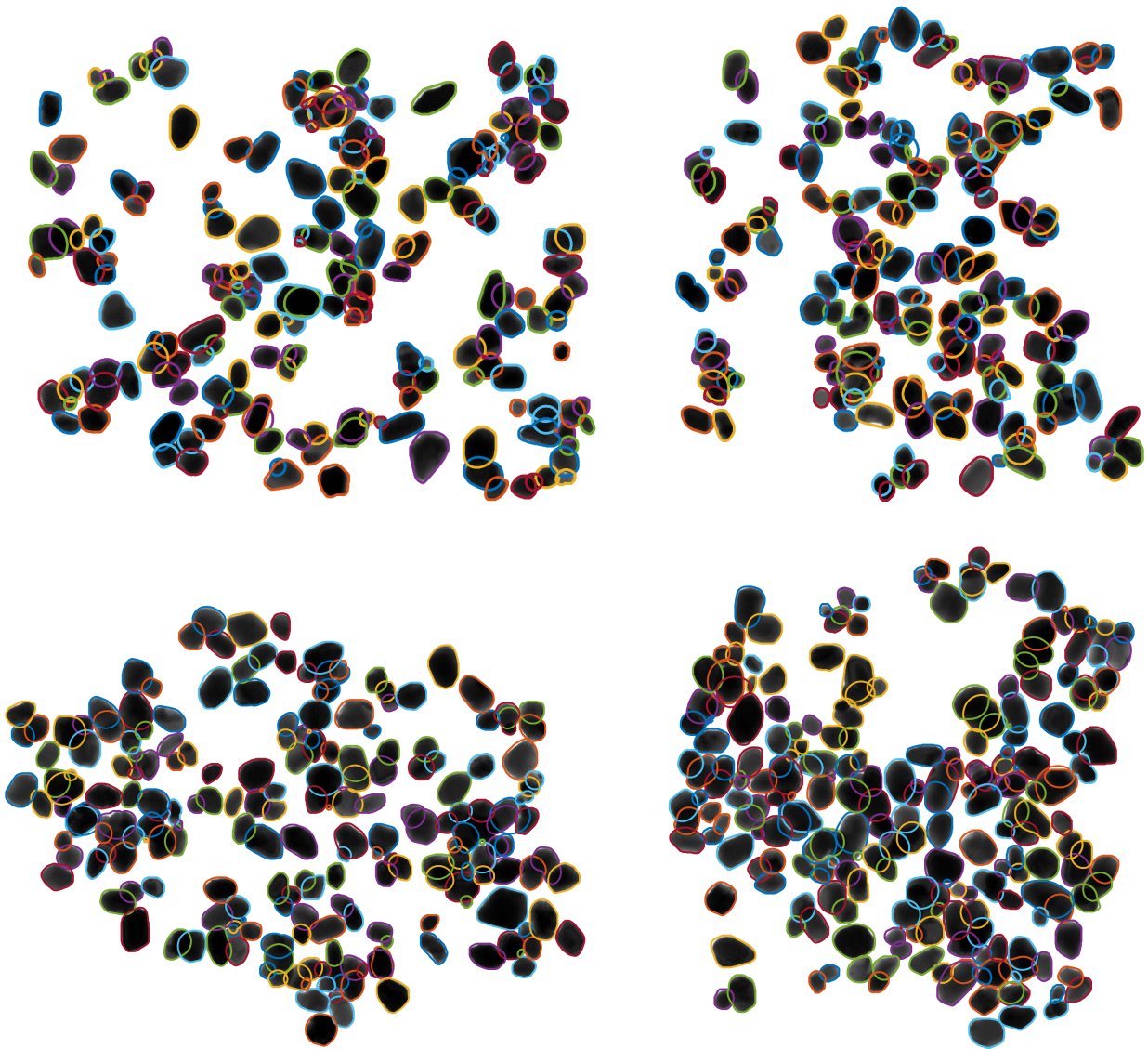


Appendix A. (continued)



(continues)

**Appendix B. Visual results of the SPGP-PF method applied to the obtained evidences**



(continues)

Appendix B. (continued)



(continues)

Appendix B. (continued)

